Ab initio simulations on the atomic and electronic structure of single-walled BN nanotubes and nanoarches

Yuri F. Zhukovskii [a], Sergei Piskunov [a,b,*], Nicola Pugno [c], Baiba Berzina [a], Laima Trinkler [a], Stefano Bellucci [d]

[a] Institute for Solid State Physics, University of Latvia, Kengaraga 8, Riga LV-1063, Latvia
[b] Lehrstuhl für Theoretische Chemie, Universität Duisburg-Essen, Universitätstraße 5, D-45141 Essen, Germany
[c] Department of Structural Engineering, Politecnico di Torino, Corso Duca degli Abruzzi 24, I-10129 Torino, Italy
[d] INFN-Laboratori Nazionali di Frascati, Via Enrico Fermi 40, I-00044 Frascati, Italy

ARTICLE INFO

ABSTRACT

To simulate the perfect single-walled boron nitride nanotubes and nanoarches with armchair- and zigzag-type chiralities and uniform diameter of ~5 nm, we have constructed their one-dimensional (1D) periodic models. In this study, we have compared the calculated properties of nanotubes with those for both hexagonal and cubic phases of bulk: bond lengths, binding energies per B–N bond, effective atomic charges as well as parameters of total and projected one-electron densities of states. For both phases of BN bulk, we have additionally verified their lattice constants. In the density functional theory (DFT), calculations performed using formalism of the localized Gaussian-type atomic functions as implemented in the CRYSTAL-06 code we have applied Hamiltonians containing either PWGGA or hybrid (DFT+HF) B3PW exchange-correlation functionals. After calculation of Hessian matrix for the optimized structures of BN bulk (both phases) and nanotubes (both chiralities) using the CRYSTAL code we have estimated their normal phonon modes within the harmonic approximation. Applying both atomistic and continuum models we have calculated the elastic energies and moduli for SW BN nanoarches. Our calculations clearly show a reproducibility of the atomic structure, effective charges and total energy, as well as phonon and elastic properties when using either PWGGA or hybrid B3PW Hamiltonians. On other hand, there is a high sensitivity of the discrete energy spectra parameters (including band gap) to the choice of the first principles approach (the hybrid method reproduce them noticeably better).

1. Introduction

Boron nitride (BN) is a synthetic III–V compound with extraordinary mechanical, thermal, electrical, optical and chemical properties widely applied for technological purposes [1]. BN is isoelectronic to the elemental forms of carbon, which results in a certain isomorphism between the two species. First BN crystalline samples were synthesized at room temperature and atmospheric pressure as structures containing hexagonal sp^2-bonded sheets isomorphic with grapheme [1,2]. Stacked as planes, they form crystalline hexagonal boron nitride (h-BN), structurally similar to graphite with the exception that hexagonal rings of the basal planes in h-BN are positioned directly above each other and rotated by 180° between alternate layers (Fig. 1a). Moreover, graphite provides a conductivity of noticeably delocalized π-electrons parallel to the honeycomb sheets, whereas the partial ionicity of h-BN makes it a semiconductor with the band gap experimentally estimated to be 5.97 eV [3]. Samples of h-BN were mainly obtained by nitridation or ammonolysis of boric acid at elevated temperature [1].

The diamond-like cubic allotrope of BN (c-BN) known as borazon (Fig. 1b) is the synthetic material with a second highest hardness and thermal conductivity next to diamond. Both c-BN and diamond are structurally similar sp^3-bonded crystals [2] acting as electrical insulators and excellent thermally stable conductors of heat with a high resistance to oxidation. The cubic boron nitride can be synthesized under the high pressure and the high temperature treatment of hexagonal boron nitride. Besides well-known c- and h-BN crystalline structures there were synthesized several metastable phases too: w-BN (wurtzite-like structure with sp^3 hybridization, which is the most thermodynamically stable for nitrides of more heavy III group metals—Al, Ga and In) [4], r-BN and t-BN (sp^2 rhombohedric and turbostratic structures, respectively) as well as amorphous a-BN [1].

* Corresponding author at: Institute for Solid State Physics, University of Latvia, Kengaraga 8, Riga LV-1063, Latvia. Tel.: +37167187480; fax: +37167132778.
E-mail address: piskunov@lu.lv (S. Piskunov).

Analogously to carbon nanotubes (CNTs), formation of BN NTs can be considered as a result of rolling up the *h*-BN (0 0 0 1) graphitic sheets, both single- and multi-walled (SW and MW, respectively) [5]. Firstly, experimental synthesis of BN NTs was performed in 1995: multi-walled nanotubes with inner diameters on the order of 1–3 nm and with lengths up to 200 nm were produced in a carbon-free plasma discharge between a BN-packed tungsten rod and a cooled copper electrode [6]. Now BN nanotubes are synthesized mainly via catalytic vapor–liquid–solid (VLS) mechanism at temperature higher than 1000 °C, using different experimental methods (arc discharge, laser ablation and chemical vapor deposition) [6–11]. Currently, the most efficient method of BN NTs production includes heating MgO (particularly doped by SnO) and B powder mixture followed by formation of B_2O_2 gas and its reaction with NH_3 [7,11]. Under certain experimental conditions not only SW and MW BN NTs but also ropes consisting of numerous SW or MW nanotubes of similar morphology were synthesized [11]. Besides synthesis of NTs, particular reconstruction observed on the edges of stacked *h*-BN (0 0 0 1) honeycomb sheets and comprising (1 $\bar{1}$ 0 0) faces results in the formation of nanoarches (NAs) between the nearest sheets

[12]. The tightest radii occur for SW NAs between the adjacent planes whereas the nested arches similar to half MW NTs can also grow. The BN NAs were grown between other surfaces of different BN phases as well [13,14]. Formation of concentric fullerene molecules containing both hexagons and non-stoichiometric pentagons was also observed experimentally during synthesis of BN nanostructures [9].

Since the mechanism of BN NTs growth is still not well defined [15], comprehensive theoretical simulations on these nanotubes continue to attract enhanced attention. Atomistic calculations on BN nanotubes were performed so far for both SW and MW models (regular, deformed and defective) characterized by the two equilibrium structures possessing either armchair (*ac*)- or zigzag (*zz*)-type chirality (Fig. 2) and a wide range of uniform diameters (0.5–2 nm) [15–28]. For modeling on BN NTs, both finite cage-like clusters (either with fullerene-like ends or H-capped) [17,18,22] and periodic one-dimensional (1D) nanotubes [5,16,19–21,23–28] were used. A number of methods were applied for their calculations: atomistic formalism of many-body empirical potentials [24], molecular dynamics [17,22], semi-empirical methods of tight-binding (TB) [16,18,20] and modified neglect of differential overlap (MNDO) [15], first principles methods of density functional theory (DFT) realized using formalisms of localized atomic functions (LCAO) [18,22,25,28] and plane waves (PW) [5,19,21,23,26,27]. In these theoretical studies parallel with the prediction of the nanotube morphology, there were analyzed the electronic structure [5,16,19,21,25–28], elastic and vibration properties [20–24], as well as thermodynamic conditions for growth of nanotubes from nuclei [15,17] and dislocation formation as a result of strain relief [22]. For example, unlike CNTs, which exhibit random chiralities in MW or ropes of SW nanotubes, a strong selection of chirality (mainly *zz*-type) was observed in BN NTs [19,28]. Some theoretical studies focus on comparison between properties of BN nanotubes of different sizes and chiralities, as well as *h*- and *c*-BN bulk (the latter were also comprehensively studied earlier) [29–33].

As to BN NAs (Fig. 3), their theoretical simulations are rather scarce present in the literature. Recently, Guerini and Piquini have performed pioneering DFT-LDA calculations on the atomic and electronic structures of single- and double-walled BN nanoarches of both armchair and zigzag types of diameter up to 1.3 nm with distinct surface helicity [13,14].

In our recent experimental studies we analyzed photoluminescence spectra of BN nanotubes and nanoarches, both MW and SW, synthesized elsewhere [10], as well as compared them with the corresponding spectra of crystalline *h*-BN and *c*-BN samples [34–36]. There was found a substantial difference in the nature of
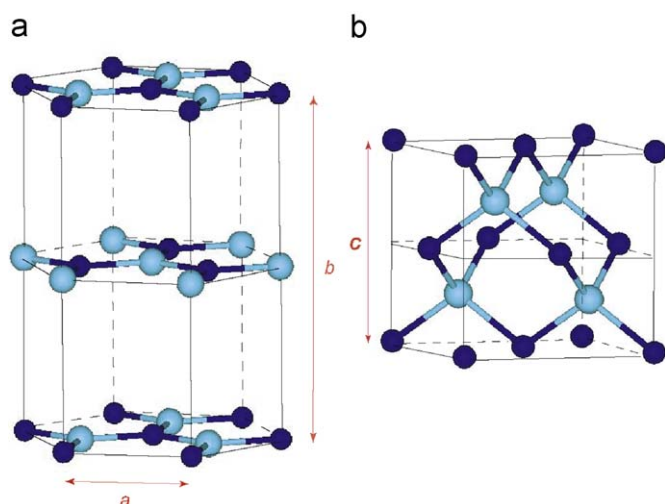

Fig. 1. Images and lattice parameters of unit cells for the two BN phases: (a) hexagonal graphite-like structure ($P6_3/mmc$ space group) and (b) zinc-blende ($F\bar{4}3m$ space group). Parameters of both BN lattices were obtained experimentally first ($a = 2.504$ Å, $b = 6.661$ Å, and $c = 3.62$ Å [1]) and then confirmed theoretically. Light turquoise balls correspond to B atoms and N atoms are shown by dark blue. (For interpretation of the references to colour in this figure legend, the reader is referred to the web version of this article.)

Fig. 2. Fragments of 5-nm-thick 1D BN nanotubes: (a) armchair-type chirality (rod symmetry Pn/m)-(36, 36) unit cell with periodicity 2.55 Å and (b) zigzag-type chirality (rod symmetry $Pnmm$)-(64, 0) unit cell with periodicity 4.45 Å. Light turquoise balls correspond to B atoms and N atoms are shown by dark blue. (For interpretation of the references to colour in this figure legend, the reader is referred to the web version of this article.)
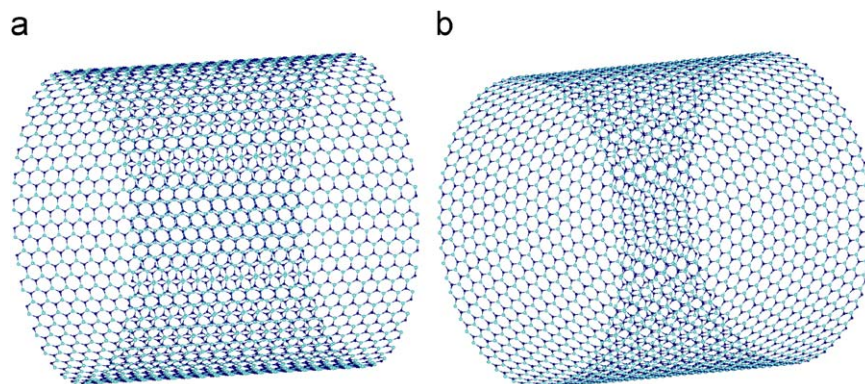
Fig. 3. Fragments of 5-nm-thick 1D BN nanoarches (halves of BN NTs extended by two fragments of parallel nanoribbons (with width of ∼1 nm each) attached to their edges: (a) armchair-type chirality-(24, 24) unit cell with periodicity 2.55 Å and (b) zigzag-type chirality-(42, 0) unit cell with periodicity 4.45 Å. Light turquoise balls correspond to B atoms and N atoms are shown by dark blue. (For interpretation of the references to colour in this figure legend, the reader is referred to the web version of this article.)
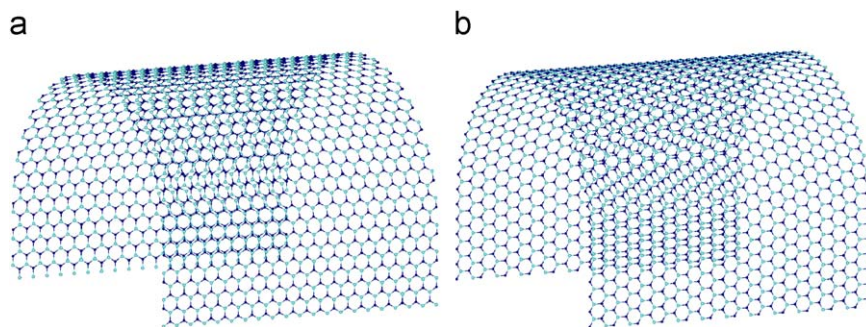
exciton luminescence observed from bulk BN samples and in that from BN NTs and NAs. In the current study, we have performed systematic first principle calculations on the atomic, electronic and phonon structure of periodic 1D BN nanostructures and those of c- and h-BN single crystals, as well as their comparative analysis and verification, using available experimental and theoretical data. Similar theoretical simulations were successfully performed by us recently, in order to study periodic 1D, 2D and 3D AlN structures, both regular [37] and defective [38]. In the current study, we have used models of SW BN NTs and NAs whose diameter (5 nm) is comparable with the minimum size of samples experimentally synthesized by our partners [10]. We also have performed comparative calculations of the harmonic frequencies for optimized 3D and 1D BN structures based on their preliminary DFT-LCAO calculations. To better analyze the elastic properties of BN NAs, we have coupled *ab initio* atomistic simulations with a continuum model based on elasticity.

The most of experimentally produced BN nanotubes were found to be defective even under conditions of their synthesis [6–11]. Recent theoretical studies on BN NTs [22,23,25,27], AlN NTs [38,39] and CNTs [40,41] clearly indicate that the defects may noticeably govern the mechanical and other properties of the system. Nevertheless, our current defect-free analysis is a prerequisite to better clarify their role and especially to calculate a wide spectrum of nanotube properties. More so because, we also simulate the single N vacancy as well as C_N and O_N substitutes upon the SW BN NTs of both chiralities [42].

2. Theoretical background

2.1. Ab initio calculations of periodic BN models and their properties

We have performed periodic DFT calculations with partial or total optimization on the two 3D models of BN bulk (Fig. 1a and b), two 1D models of single-walled BN nanotubes (Fig. 2a and b) and two 1D models of single-walled BN nanoarches (Fig. 3a and b), using formalism of the localized Gaussian-type functions (GTFs) as implemented in the *CRYSTAL-06* code [43]. Concerning NAs, we have used previously optimized structure of halves of the corresponding NTs then relaxing only the structure of attached nanoribbons (Fig. 3). To perform *ab initio* calculations, we have applied the DFT Hamiltonians containing either exchange-correlation functional PWGGA [44] (Perdew–Wang generalized gradient approximation used for both exchange and correlation) or hybrid B3PW [45] (i.e., DFT-Becke and exact Hartree-Fock exchange operators mixed in certain ratio plus PWGGA correlation). The all-valence basis sets for B and N GTFs ($6s$–$21sp$–$1d$ and $6s$–$31p$–$1d$, respectively) were optimized

elsewhere (for B-containing crystalline compounds [46] and various nitrides [47]), therefore we only slightly have re-optimized their valence and virtual shells.

To provide the balanced summation over the direct and reciprocal lattices, the reciprocal space integration has been performed by sampling the Brillouin zone (BZ) with the $8 \times 8 \times 8$ Pack–Monkhorst k-mesh [48] and 8 for Gilat k-mesh [49] in the case of BN bulk, while $4 \times 1 \times 1$ Pack–Monkhorst k-mesh has been adopted in simulations on BN NTs and NAs. The threshold parameters of *CRYSTAL* code (ITOLn) for evaluation of different types of bielectronic integrals (overlap and penetration tolerances for Coulomb integrals, ITOL1 and ITOL2, overlap tolerance for exchange integrals ITOL3, as well as pseudo-overlap tolerances for exchange integral series, ITOL4 and ITOL5) [43] have been set to 8, 8, 8, 8, and 16, respectively. (If the overlap between the two atomic orbitals is smaller than $10^{-\text{ITOLn}}$, the corresponding integral is truncated.) Further increasing of k-mesh and threshold parameters results in much more expensive calculations yielding only a negligible gain in the total energy ($\sim 10^{-6}$ a.u.). Calculations are considered as converged when the total energy obtained in the self-consistent field procedure differs by less than 10^{-7} a.u. in the two successive cycles.

When performing the optimization of bulk structures shown in Fig. 1 we have fixed their symmetry and have changed only their optimized lattice parameters: two (a and b) for the hexagonal structure and one (c) for the cubic structure. The B–N bond length, which results in the change of the corresponding nanotube and nanoarch diameters, has been optimized as well. For 3D and 1D models shown in Figs. 1–3, we have determined the binding energy *per* B–N pair and the charge transfer along it (Table 1). For the former, we have used the following expression:

$$E_{bind}(\text{B}-\text{N}) = \frac{E_{tot}(\text{unit cell of BN model})}{n_{\text{BN}}} - E_{tot}(\text{BN molecule}),$$

(1)

where E_{tot} is the calculated total energy *per* molecule or unit cell and n_{BN} the number of BN pairs *per* unit cell. Parameters of the atomic and electronic structure of 3D and 1D periodic BN systems are analyzed in Section 3.

Procedure of harmonic frequency calculation in periodic systems at the Γ point of Brillouin Zone is firstly implemented in the last edition of *CRYSTAL* code [43]. For this purpose, the geometry of the system must correspond to a stationary point on the potential energy surface preliminary defined by optimizing the periodic structure. Total energy calculations to compute numerical derivatives are carried out exploiting the residual symmetry of the system after displacement. The second derivatives of the energy (elements of Hessian matrix $\|H\|$ [50]) are computed numerically by using the analytical first derivatives

Table 1
The structural and electronic properties calculated for perfect BN bulk and NTs.

Feature	Method	Bulk		SW nanotube	
		h-Type	c-Type	Armchair	Zigzag
d_{B-N} (Å)	B3PW	1.446	1.565	1.444	1.447
	PWGGA	1.453	1.573	1.453	1.453
	Literature	1.45 [1]	1.57 [1]	1.44-1.45 [24]	
E_{bind}(B–N) (eV)	B3PW	10.07	10.02	10.04	10.09
	PWGGA	9.86	9.71	9.75	9.75
	Literature	8.8–13.0 [32]	–[a]		
Δq_B (Δq_N) (E)	B3PW	±0.98	±1.15	±0.99	±0.97
	PWGGA	±0.84	±1.05	±0.82	±0.82
	Literature	±0.9–1.2 [30,32]	–[a]		
$\Delta\varepsilon_{gap}$ (ε_F) (eV)	B3PW	6.60	6.20	6.94	6.57
	PWGGA	4.79	4.50	5.13	4.78
	Literature	4.0–6.4[b]	3.2–5.5[b]		

[a] The corresponding experimental data were not found in the literature.
[b] These ranges of band gaps cover the wide spectra of results obtained in numerous studies.

[43]. The vibrational frequencies at the Γ point of Brillouin zone can be obtained by diagonalizing the dynamical mass-weighted matrix $\|D\|$ with the elements $D_{AB} = H_{AB}/\sqrt{M_A M_B}$, where M_A and M_B are the masses of A and B atoms, respectively. Analysis of normal modes (eigenvectors) [51] and harmonic frequencies of BN structures is performed in Section 4.

2.2. Elastic calculations on continuum and atomistic models of nanoarches

Predictions based on classical continuum elasticity seem to work for nanotubes and nanoarches as suggested by finite element simulations [52]. Let us model the curved graphene sheet (nanoarch) as a linear elastic isotropic continuum plate, having elastic modulus E, Poisson's ratio ν and thickness t. If we impose the bending curvatures $\chi_{x,y}$ as well as a torsion curvature χ_{xy}, the classical theory of plates [53] would predict the following bending ($\sigma_{x,y}$) and torsion (σ_{xy}) stresses:

$$\sigma_x(z) = \frac{E}{1-\nu^2}(\chi_x + \nu\chi_y)z, \quad \sigma_y(z) = \frac{E}{1-\nu^2}(\chi_y + \nu\chi_x)z,$$
$$\sigma_{xy}(z) = G\chi_{xy}z, \tag{2}$$

where $G = E/(2(1+\nu))$ is the shear modulus of elasticity, ν the Poisson ratio and $-t/2 \leqslant z \leqslant +t/2$ the perpendicular coordinate, along the plate thickness t. The elastic energy W per unit area A, W/A, can be calculated from the complementary elastic potential D as

$$\frac{W}{A} = \int_{-t/2}^{+t/2} D(z)dz;$$
$$D(z) = \frac{1}{2E}(\sigma_x^2(z) + \sigma_y^2(z)) - \frac{\nu}{E}\sigma_x(z)\sigma_y(z) + \frac{1}{2G}\sigma_{xy}^2(z). \tag{3}$$

The developed procedure can be now applied to calculate the maximum stress and stored elastic energy in the nanoarch under pure uniaxial bending, i.e., $\chi_x = 1/R$, $\chi_y = \chi_{xy} = 0$, where R is the imposed radius of curvature. We accordingly deduce a maximum stress of:

$$\sigma_{x\,max} = \frac{Et}{2(1-\nu^2)R} \tag{4}$$

(note that $\sigma_y = \nu\sigma_x$ also exists) and a stored elastic energy per unit area of

$$\frac{W}{A} = \frac{Et^3}{24(1-\nu^2)R^2}. \tag{5}$$

Predicted stress and energy are reported in Section 4 (Table 3) for models of BN NAs (Fig. 3).

Atomistic simulations of elastic properties confirm analogous finding. In particular, when examining the energies of several SW CNTs with radii less than 0.9 nm it was found that the NTs possess the internal strain energy per carbon atom (relative to an unstrained graphite sheet) with $1/R^2$ dependence, even down to radii of 0.35 nm, in agreement with the prediction of continuum elasticity [54]. This was subsequently confirmed in several studies [55–58], i.e., that SW CNTs and BN NTs follow the behavior expected from classical elasticity theory. These calculations indicate that the estimated maximum stress will take place in the nanotube. We may also note that our computed maximum stresses are in the expected range of GPa units [59]. The Poisson ratio is defined in this case from the following relation:

$$\frac{R - R_{eq}}{R_{eq}} = -\nu\xi, \tag{6}$$

where ξ is the axial strain, R_{eq} is the equilibrium radius, and R is the radius at strain ξ. Young modulus is calculated from its conventional definition:

$$E = \frac{1}{V_0}\frac{\partial^2 W}{\partial\xi^2}\bigg|_{\xi=0}, \tag{7}$$

where V_0 is the equilibrium volume and W is the calculated strain energy. The values of E and ν obtained for nanoarches considered in this study are reported in Section 4 (Table 3).

3. Atomic and electronic structure

In this section, we analyze the calculated structural and electronic properties for different morphologies of boron nitride bulk, nanotubes and nanoarches (Table 1 and Figs. 4 and 5) comparing them also with available experimental and theoretical data obtained earlier for the same species. According to our calculations, optimized lattice constants for h-BN and c-BN structures have been found to be very close to the corresponding experimental data mentioned in caption of Fig. 1: a (hereafter 2.51 Å in B3PW and 2.52 Å in PWGGA calculations vs. 2.50 Å obtained in experiment [1]), b (7.0, 6.9 vs. 6.7 Å), and c (3.61, 3.63 vs. 3.62 Å). Thus, for direct comparison of different structures, we consider only the nearest B–N distances. Results presented in Table 1 show a certain difference between the properties of both BN phases confirmed by data available in the literature. Moreover, except for parameters of the density of states (DOS), it is observed rather a qualitative proximity between the values of bond length, d_{B-N}, binding energy per bond, E_{bind}(B–N) and effective (Mulliken) atomic charges, $\Delta q_{B(N)}$, calculated for the same structure using both B3PW and PWGGA methods. The noticeable difference between the corresponding values of d_{B-N} and $\Delta q_{B(N)}$ for h- and c-BN bulk structures can be explained by difference in both B–N bonding (sp^2 and sp^3, respectively) and space charge distribution. In particular, for c-BN phase, the bond ionicity [30] is larger as compared to h-BN whereas its covalency is smaller. The maximum of electron density in BN is localized close to the midpoint along the covalent bond [32], which can be explained by proximity of ionic radii of the B and N atoms as a result of the electronic charge transfer.

When comparing the difference between the values of d_{B-N} and $\Delta q_{B(N)}$ for nanotubes of various chiralities, it has been found to be noticeably smaller than between the different phases of BN bulk since due to a large diameter of BN NT the sp^2 hybridization remains practically unchanged in both types of nanostructures, irrespective of the morphology [5,26]. A certain quantitative
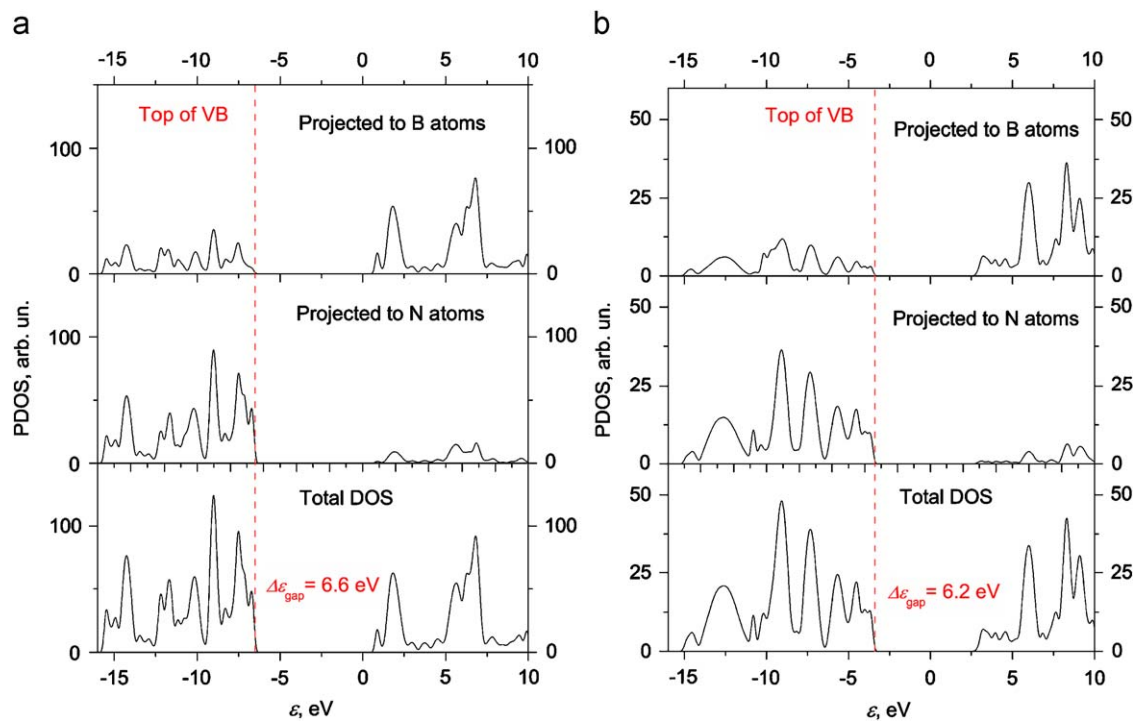
Fig. 4. Total and projected densities of one-electron states (DOSs) for (a) *h*-BN (Fig. 1(a)) and (b) *c*-BN (Fig. 1(b)) bulk calculated using hybrid B3PW Hamiltonian [43]. Details of DOSs are described inside the plots; moreover, values of $\Delta\varepsilon_{gap}$ are also presented in Table 1. (For interpretation of the references to colour in this figure legend, the reader is referred to the web version of this article.)
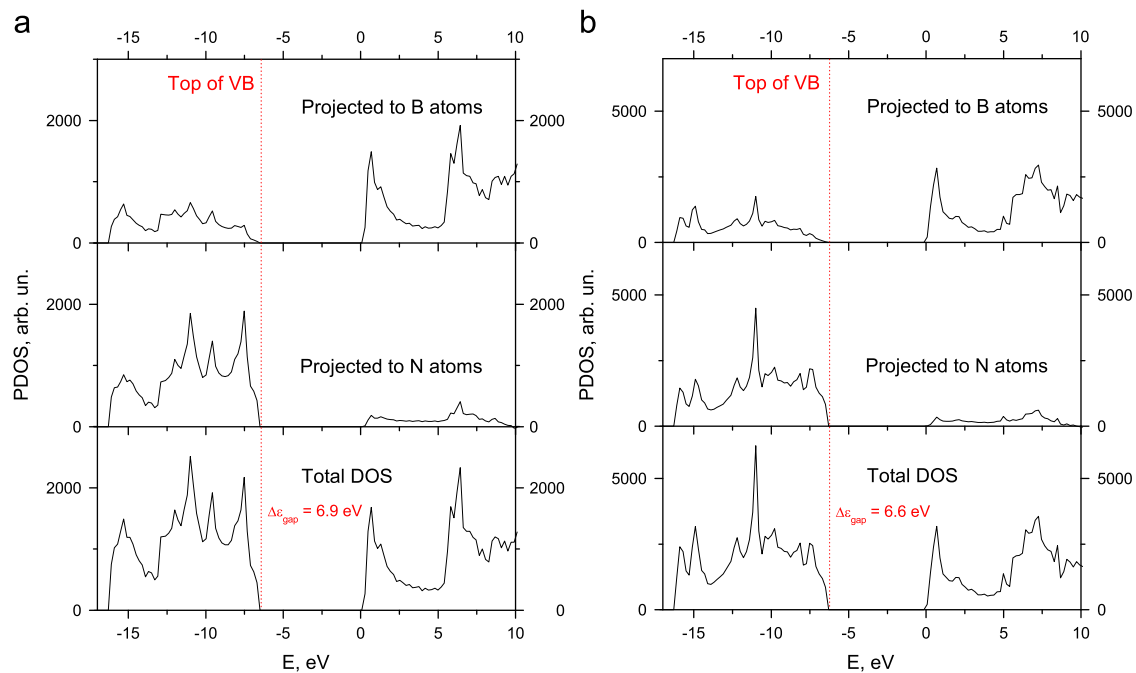

Fig. 5. The total and projected densities of one-electron states (DOSs) for BN NTs: (a) 5 nm armchair-type (36, 36) (Fig. 2(a)) and (b) 5 nm zigzag-type (64, 0) (Fig. 2(b)). For details, see explanations given in Fig. 4. (For interpretation of the references to colour in this figure legend, the reader is referred to the web version of this article.)

proximity is observed between the d_{B-N} and $\Delta q_{B(N)}$ values for *h*-BN and NT structures, which possess such a large diameter (5 nm) described by the same sp^2 nature of B–N bonding (Table 1). Nevertheless, for BN NTs of smaller diameter, some contribution from the sp^3 bonding also takes place, thus increasing the difference between the properties of both *h*-BN and BN NTs [5].

Substantial difference between the results of calculations performed using the PWGGA and B3PW methods on different BN structures presented in Table 1 and Figs. 4 and 5 is observed for the total and atom-projected DOSs including the band gap ($\Delta\varepsilon_{gap}$). Obviously, most of pure DFT calculations on the band gaps performed for BN structures so far noticeably underestimated $\Delta\varepsilon_{gap}$, down to 4.0–5.0 eV [5,19,25–27,33] whereas Hartree–Fock

(HF) calculations usually markedly overestimated it [32]. Hence, we have compared the corresponding results calculated using the hybrid B3PW method [45], which usually reproduce the band gap well, and the DFT PWGGA Hamiltonian [44] often used earlier for simulations on 1D nanostructures. The DOSs presented in Figs. 4 and 5 contain results of B3PW calculations only since values of $\Delta\varepsilon_{gap}$ for BN bulk and BN NTs are much closer to those obtained in experiments (5.5–6.0 eV) although somewhat exceed them. (Nevertheless, the profiles of the corresponding DOS bands for the same structures are rather similar when using both methods.)

Different nature of the B–N bonding in h-BN and c-BN bulk (sp^2 and sp^3, respectively) also leads to the difference between their DOSs (Fig. 4) and other parameters of the electronic structure (Table 1). Unlike the optical band gap energies recently measured experimentally (5.96 vs. 6.36 eV for a hexagonal and cubic structures of BN bulk, respectively [60]), we have obtained the larger band gap for the hexagonal structure (minimum at the K point of BZ) vs. the smaller value of $\Delta\varepsilon_{gap}$ for c-BN (at the X point of BZ) as shown in Fig. 4 and Table 1. A possible reason of mismatch between the parameters of energy spectra for BN bulk, both simulated theoretically and measured experimentally, can be a presence of defects or surface disturbances within the sample [61]. Moreover, one could suppose the coexistence of cubic and hexagonal domains within the same sample.

Detailed qualitative analysis of the total and atom-projected DOS for both ac- and zz-BN NTs was recently performed elsewhere [26]. The single-walled zz-BN$(n,0)$ NT (Fig. 2(b)) is a direct band gap nanostructure. It has been found that N(2s) electrons are mainly localized at the interval between -19 to -13 eV (Fig. 5), especially when n is as large as in our study (64). The latter also leads to both a broadening of DOS bands and their particular overlap. Due to the difference in electronegativity between the N and B atoms (according to Pauling scale: 2.04/B and 3.04/N [26]), the VB and CB are contributed by the occupied N(2p_z) and the unoccupied B(2p_z) orbitals, respectively, which result in prevailing of BN molecular orbitals π and π^*, respectively. The B(2s) states also contribute in this energy interval, especially at the bottom of CB. In contrast to zz-chirality, the single-walled ac-BN(36, 36) NT possesses an indirect band gap in the range of smaller values of $\Delta\varepsilon_{gap}$ as compared to zz-BN NT (Fig. 5). Similar to zz-BN NT, N(2s) electrons are mainly local at the same interval -19 to -13 eV while B(2s) electrons are well delocalized around the band gap. Analogous effects have been also observed for contribution of both N(2p_z) and B(2p_z) states to the top of VB and bottom of CB, respectively.

4. Vibrational and elastic structure

Using both B3PW and PWGGA methods for DFT calculations as well as applying a procedure of harmonic frequencies calculations as implemented in CRYSTAL-06 code [43] and briefly described in Section 2.1 there have been calculated and experimentally verified [29] three transversal-optical (TO) phonon modes for h-BN bulk active in infra-red (IR) spectra: A_{2u} and $2E_{1u}$ (Table 2). For c-BN bulk, the IR-active TO mode T_2 has been analogously calculated

and verified [31]. Obviously, we can ascertain the qualitative accordance of vibrational frequencies and their spectral intensities for h-BN and c-BN bulk phases, both calculated in the current study and experimentally measured previously [29,31]. It is well observed that the hybrid B3PW calculations result in systematically larger values of wavenumbers as compared to the PWGGA DFT calculations, i.e., there exists some correlation between the parameters of the electronic and vibrational spectra calculated using different first principles methods. Simultaneously, results of these calculations can be also considered as a successful test for further large-scale calculations and predictions of TO phonon modes for BN nanotubes since their precise experimental measurements are mainly in progress.

For ac- and zz-BN NTs (Figs. 6 and 7), we have analogously calculated the IR-active TO phonon modes, their wavenumbers and intensities. Morphology of spectra for both chiralities is more complicated as compared to those for BN bulk, especially for the latter, rather due to a lower symmetry of phonon structure in nanotubes. The most comprehensive theoretical simulations of the phonon structure in BN NTs performed so far were based on preliminary calculations using both the non-orthogonal tight-binding (TB) [20] and plane-wave LDA DFT [21] methods with further construction of the force-constant matrix. Diameters of BN nanotubes of both chiralities were consequently increased in those studies from 0.5 to 2.0 nm. Our results are better correlated with those calculated using TB method [20] where for ac-BN NT, wavenumbers of IR-active A_u mode converged to 1410 cm^{-1}, whereas first, second, and third E_{1u} modes converged to 1420, 760, and <100 cm^{-1}, respectively (cf. the corresponding modes shown in Fig. 6). For zz-BN NT, convergence of IR-active A_1 and E_1 modes with increasing diameter of nanotube was found to be worse as compared to ac-chirality [20]: 1410, 755, and 190 cm^{-1} for the former vs. 1430, 750, 230, and 130 cm^{-1} for the latter. The LDA calculations on IR-active frequencies of zz-BN NT lead to the following results [21]: 1390, 820, and 220 cm^{-1} (A_1) vs. 1420, 810, 310, and 190 cm^{-1} (E_1) (cf. the corresponding modes shown in Fig. 7). When theoretical models, which use different computational approaches, lead to close results, it means that they can be considered as qualitatively reliable. Moreover so because, our calculations on phonon modes for BN bulk are well verified by experimental results [29,31]. This is why the simulation of vibrational structure is one of the most prospective ways for effective comparison with the corresponding experimental data.

The phonon structure of BN nanotubes is well correlated with their elastic structure [62]. The elastic properties of BN NAs described in Section 2.2 and calculated in the current study are presented in Table 3. Although the corresponding data are qualitatively close, they depend on both the chirality of nanoarches and the computational method used. The magnitudes of Young modulus (E) calculated using Eq. (7) for atomistic models presented in Fig. 3 are in a qualitative agreement with the experimental value of 1220 GPa measured for MW BN NTs (being noticeably smaller than 4000 GPa for SW CNTs and drastically larger than 87 GPa for h-BN bulk) [62]. Their proximity confirms reliability of atomistic and continuum models for both description and prediction of elastic properties for BN nanostructures (Table 3).

5. Conclusions

In this study we discuss results of first principles calculations on the single-walled 5-nm-thick BN nanotubes and nanoarches possessing the two different chiralities (armchair- and zigzag-type) as well as two phases (c- and h-) of BN bulk. We analyze and compare their structural and electronic properties as well as

Table 2
Frequencies (cm^{-1}) of IR active TO phonon modes for h- and c-phases of BN bulk calculated using B3PW and PWGGA methods.

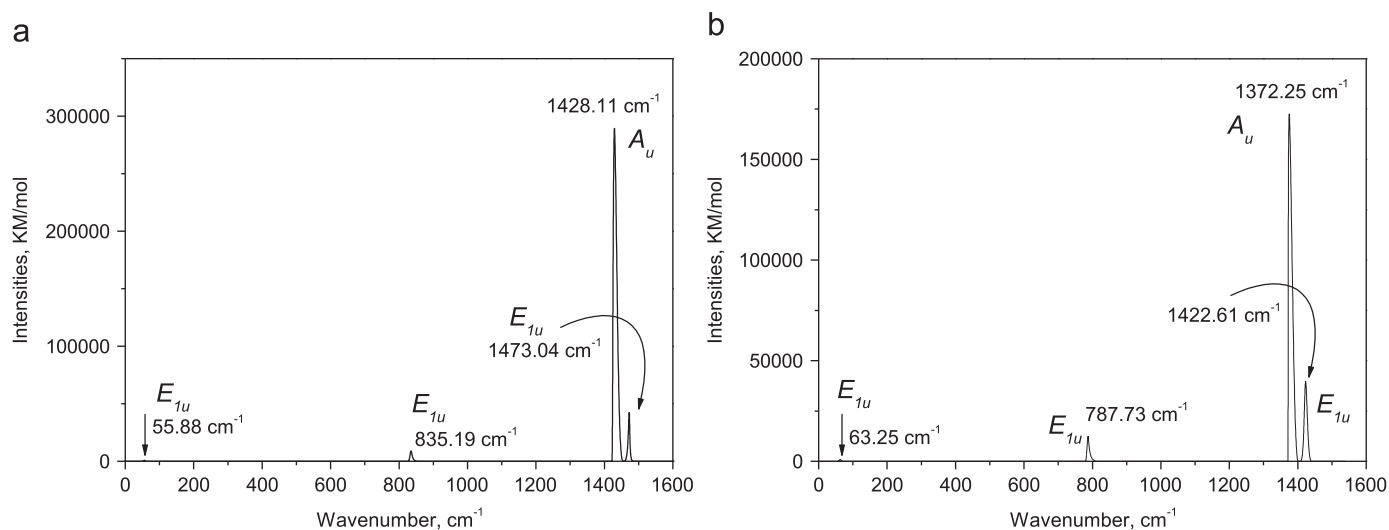| Phase	Mode	B3PW	PWGGA	Experiment [29,31]
h-BN	A_{2u}	711	652	783
	E_{1u}	1410	1371	1367
c-BN	T_2	1076	1037	1056

a

b

Fig. 6. Frequencies and intensities of IR active TO phonon mode for ac-BN NT calculated using B3PW (a) and PWGGA (b) methods.
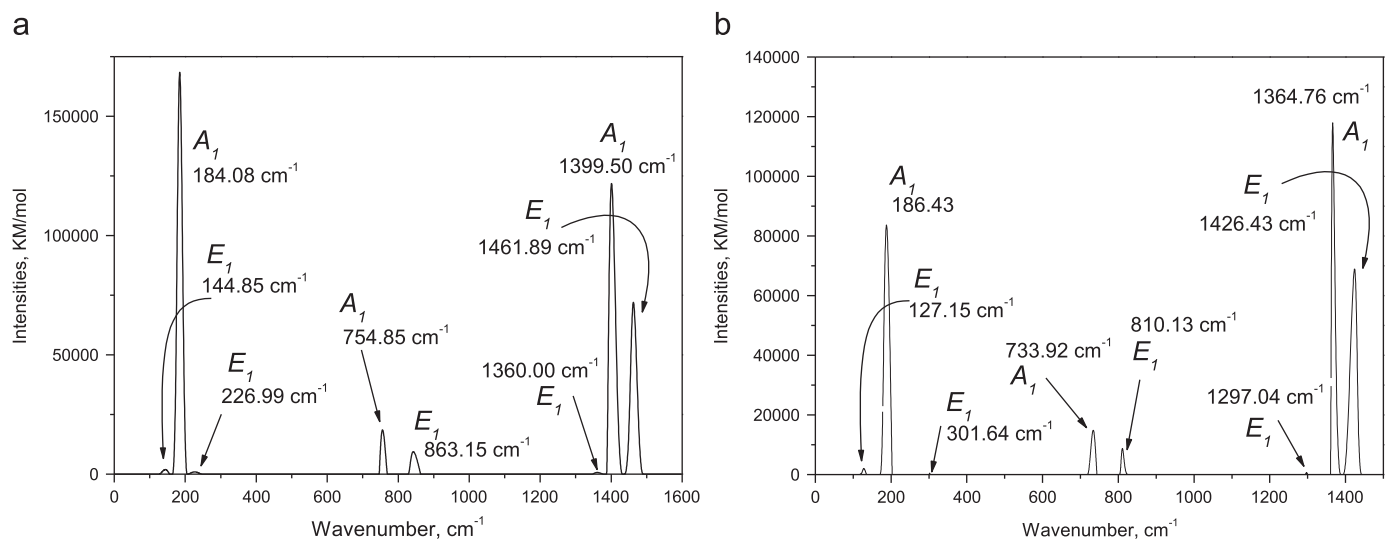
a

b

Fig. 7. Frequencies and intensities of IR active TO phonon mode for zz-BN NT calculated using B3PW (a) and PWGGA (b) methods.

Table 3

Equilibrium radius of nanoarch, $R^{(A)}$, plate thickness, $t^{(A)}$, Young modulus, $E^{(A)}$, Poisson ratio, $\nu^{(A)}$, as obtained from atomistic calculations (superscript $^{(A)}$) as well as maximum stresses, $\sigma_{x\max}^{(C)}$, and energy density, $(W/A)^{(C)}$, in continuum model (superscript $^{(C)}$), for both types of nanoarches and calculation methods considered.

Method$^{(A,C)}$/type of BN NA	Plate	B3PW/ac	PWGGA/ac	B3PW/zz	PWGGA/zz
$R^{(A)}$ (Å)	∞	24.81	24.96	25.52	25.64
t, (Å; Eq. (2))	3.33	3.33	3.33	3.33	3.33
$E^{(A)}$ (GPa; Eq. (7))	0	1000	950	889	1028
$\nu^{(A)}$ (Eq. (2))	0	0.221	0.226	0.222	0.230
$\sigma_{x\max}^{(C)}$ (GPa; Eq. (3))	0	70.56	66.78	61.01	70.48
$(W/A)^{(C)}$ (GPa Å; Eq. (4))	0	2.63	2.47	2.21	2.54

vibrational and elastic structure, verifying them with available literature data. Although a certain difference exists between the parameters of one-electron spectra of states (DOS) calculated using the B3PW and PWGGA DFT methods, other structural, vibrational, and elastic properties are described qualitatively similar. Obviously, the hybrid B3PW method is found to be more reliable for the simulation of the whole spectrum of properties for BN bulk and nanostructures.

Careful theoretical study of BN nanostructures is necessary not only for reliable comparison with the corresponding experimental data but also for proper description and even prediction for some of them (firstly, the phonon and elastic structure of BN nanotubes and nanoarches). Our recent experimental IR measurements on h-BN and BN NT samples have qualitatively confirmed the spectra predicted in this study. Additional advantage of the current study is that we present results

obtained using a combination of two different complimentary theoretical approaches using atomistic and continuum models.

Acknowledgments

References

[1] R. Haubner, M. Wilhelm, R. Weissenbacher, B. Lux, in: High Performance Non-Oxide Ceramics II, Series Structure and Bonding, vol. 102, Springer, Berlin, Heidelberg, New York, 2002, pp. 1–45.
[2] P.B. Mirkarimi, K.F. McCarty, D.L. Medlin, Mater. Sci. Eng. R 21 (1997) 47–100.
[3] K. Watanabe, T. Taniguchi, H. Kanda, Nat. Mater. 3 (2004) 404–409.
[4] P. Ruterana, M. Albrecht, J. Neugebauer, Nitride Semiconductors: Handbook on Materials and Devices, Wiley Interscience, New York, 2003.
[5] X. Blasé, A. Rubio, S.G. Louie, M.L. Cohen, Europhys. Lett. 28 (1994) 335–340.
[6] N.G. Chopra, R.J. Luyken, K. Cherrey, V.H. Crespi, M.L. Cohen, S.G. Louie, A. Zettl, Science 269 (1995) 966–967.
[7] D. Golberg, Y. Bando, M. Eremets, K. Takemura, K. Kurashima, H. Yusa, Appl. Phys. Lett. 69 (1996) 2045–2047.
[8] A. Loiseau, F. Willaime, N. Demoncy, G. Hug, H. Pascard, Phys. Rev. Lett. 76 (1996) 4737.
[9] E. Bengu, L.D. Marks, Phys. Rev. Lett. 86 (2001) 2385.
[10] R. Czerw, S. Webster, D.L. Carroll, S.M.C. Vieira, P.R. Birkett, C.A. Rego, S. Roth, Appl. Phys. Lett. 83 (2003) 1617–1619.
[11] D. Golberg, M. Mitome, Y. Bando, C.C. Tang, C.Y. Zhi, Appl. Phys. A 88 (2007) 347–352.
[12] L. Nistor, V. Teodorescu, C. Ghica, J. Van Landuyt, G. Dinca, P. Georgeoni, Diamond Relat. Mater. 10 (2001) 1352–1356.
[13] S. Guerini, P. Piquini, Surf. Sci. 71 (2004) 179–186.
[14] S. Guerini, V. Lemos, P. Piquini, Nanotechnology 17 (2006) 556–560.
[15] V.L. Kuznetsov, I.N. Mazov, A.I. Delidovich, E.D. Obraztsova, A. Loiseau, Phys. Status Solidi (B) 244 (2007) 4165–4169.
[16] A. Rubio, J.L. Corkill, M.L. Cohen, Phys. Rev. B 49 (1994) 5081–5084.
[17] X. Blasé, A. De Vita, J.-C. Charlier, R. Car, Phys. Rev. Lett. 80 (1998) 1666–1669.
[18] P.W. Fowler, K.M. Rogers, G. Seifert, M. Terrones, H. Terrones, Chem. Phys. Lett. 299 (1999) 359–367.
[19] Y.H. Kim, K.J. Chang, S.G. Louie, Phys. Rev. B 63, 205408.
[20] D. Sánchez-Portal, E. Hernández, Phys. Rev. B 66 (2002) 235415.
[21] H.J. Xiang, J. Yang, J.G. Hou, Q. Zhu, Phys. Rev. B 68 (2003) 035427.
[22] T. Dumitrică, H.F. Bettinger, G.E. Scuseria, B.I. Yakobson, Phys. Rev. B 68 (2003) 085412.
[23] Y. Miyamoto, A. Rubio, S. Berber, M. Yoon, D. Tománek, Phys. Rev. B 69 (2004) 121413.
[24] W.H. Moon, H. Hwang, Physica E 23 (2004) 26–30.
[25] P. Piquini, R.J. Baierle, T.M. Schmidt, A. Fazzio, Nanotechnology 16 (2005) 827–831.
[26] J.F. Jia, H.S. Wu, H. Jiao, Physica B 381 (2006) 90–95.
[27] A. Zobelli, C.P. Ewels, A. Gloter, G. Seifert, O. Stephan, S. Csillag, C. Colliex, Nano Lett. 6 (2006) 1955–1960.
[28] S. Guerini, V. Lemos, P. Piquini, S.S. Coutinho, Phys. Status Solidi (B) 244 (2007) 110–115.
[29] R. Geick, C.H. Perry, G. Rupprecht, Phys. Rev. 146 (1966) 543–547.
[30] N.E. Christensen, S. Satpathy, Z. Pawlowska, Phys. Rev. B 36 (1987) 1032–1050.
[31] T.A. Friedmann, P.B. Mirkarimi, D.L. Medlin, K.F. McCarty, E.J. Klaus, D.R. Boehme, H.A. Johnsen, M.J. Mills, D.K. Ottesen, J.C. Barbour, J. Appl. Phys. 76 (1994) 3088–3101.
[32] A. Lichanot, P. Azavant, U. Pietsch, Acta Crystallogr. B 52 (1996) 586–595.
[33] L.E. Ramos, L.K. Teles, L.M.R. Scolfaro, J.L.P. Castineira, A.L. Rosa, J.R. Leite, Phys. Rev. B 63 (2001) 165210.
[34] B. Berzina, L. Trinkler, K. Atobe, Phys. Status Solidi (C) 0 (2002) 421–424.
[35] B. Berzina, L. Trinkler, R. Krutohvostov, R.T. Williams, D.L. Carroll, R. Czerw, E. Shishonok, Phys. Status Solidi (C) 2 (2005) 318–321.
[36] B. Berzina, L. Trinkler, V. Korsak, R. Krutohvostov, D.L. Carroll, K.B. Ucer, R.T. Williams, Phys. Status Solidi (B) 243 (2006) 3840–3845.
[37] Yu.F. Zhukovskii, A.I. Popov, C. Balasubramanian, S. Bellucci, J. Phys.: Condens. Matter 18 (2006) S2045–S2054.
[38] Yu.F. Zhukovskii, N. Pugno, A.I. Popov, C. Balasubramanian, S. Bellucci, J. Phys.: Condens. Matter 19 (2007) 395021.
[39] M. Simeoni, S. Santucci, S. Picozzi, B. Delley, Nanotechnology 17 (2006) 3166–3174.
[40] J. Kotakoski, A.V. Krasheninnikov, K. Nordlund, Phys. Rev. B 74 (2006) 245420.
[41] A.R. Rocha, M. Rossi, A. Fazzio, A.J.R. da Silva, Phys. Rev. Lett. 100 (2008) 176803.
[42] Yu.F. Zhukovskii, S. Bellucci, S. Piskunov, L. Trinkler, B. Berzina, Eur. Phys. J. B 67 (2009) 519–525.
[43] R. Dovesi, V.R. Saunders, C. Roetti, R. Orlando, C.M. Zicovich-Wilson, F. Pascale, B. Civalleri, K. Doll, N.M. Harrison, I.J. Bush, Ph. D'Arco, M. Llunell, CRYSTAL-2006 User Manual, University of Turin, 2006.
[44] J.P. Perdew, J.A. Chevary, S.H. Vosko, K.A. Jackson, M.R. Pederson, D.J. Singh, C. Fiolhais, Phys. Rev. B 46 (1992) 6671–6687.
[45] A.D. Becke, J. Chem. Phys. 98 (1993) 5648–5652.
[46] R. Orlando, R. Dovesi, C. Roetti, J. Phys.: Condens. Matter 2 (1990) 7769–7789.
[47] C. Gatti, V.R. Saunders, C. Roetti, J. Chem. Phys. 101 (1994) 10686–10696.
[48] H.J. Monkhorst, J.D. Pack, Phys. Rev. B 13 (1976) 5188–5192.
[49] G. Gilat, Phys. Rev. B 26 (1982) 2243–2246.
[50] R. Lindh, A. Bernhardsson, G. Katlström, P.A. Malmqvist, Chem. Phys. Lett. 241 (1995) 423–428.
[51] F. Pascale, C.M. Zicovich-Wilson, F. Lopez, B. Civalleri, R. Orlando, R. Dovesi, J. Comput. Chem. 25 (2004) 888–897.
[52] A. Pantano, D.M. Parks, M.C. Boyce, J. Mech. Phys. Sol. 52 (2004) 789–821.
[53] A. Carpinteri, Structural Mechanics: A Unified Approach, Chapman & Hall, London, 1997.
[54] D.H. Robertson, D.W. Brenner, J.W. Mintmire, Phys. Rev. B 45 (1992) 12592–12595.
[55] J.P. Lu, Phys. Rev. Lett. 79 (1997) 1297–1300.
[56] E. Hernández E, C. Goze, P. Bernier, A. Rubio, Phys. Rev. Lett. 80 (1998) 4502–4505.
[57] X. Zhou, J.J. Zhou, Z.C. Ou-Yang, Phys. Rev. B 62 (2000) 13692.
[58] L. Vaccarini, C. Goze, L. Henrard, E. Hernández, P. Bernier, A. Rubio, Carbon 38 (2000) 1681–1690.
[59] N. Pugno, J. Phys.: Condens. Matter 18 (2006) S1971–S1990.
[60] D.A. Evans, A.G. McGlynn, B.M. Towlson, M. Gunn, D. Jones, T.E. Jenkins, R. Winter, N.R.J. Poolton, J. Phys.: Condens. Matter 20 (2008) 075233.
[61] G. Cappellini, G. Satta, M. Palummo, G. Onida, Comput. Mater. Sci. 22 (2001) 78–80.
[62] N.G. Chopra, A. Zettl, Sol. State. Commun. 105 (1998) 297–300.